

# A substantial increase of Curie temperature in a new type of diluted magnetic semiconductors via effects of chemical pressure

Shuang Yu<sup>1,2</sup>, Guoqiang Zhao<sup>1,2</sup>, Yi Peng<sup>1,3</sup>, Xiaohong Zhu<sup>3</sup>, Xiancheng Wang<sup>1,2</sup>, Jianfa Zhao<sup>1,2</sup>, Lipeng Cao<sup>1,2</sup>, Wenmin Li<sup>1,2</sup>, Zhi Li<sup>4,a)</sup>, Zheng Deng<sup>1,2,b)</sup>, and Changqing Jin<sup>1,2,5,c)</sup>

<sup>1</sup> Beijing National Laboratory for Condensed Matter Physics, and Institute of Physics, Chinese Academy of Sciences, Beijing 100190, China

<sup>2</sup> School of Physics, University of Chinese Academy of Sciences, Beijing 100190, China

<sup>3</sup> Department of Materials Science & Engineering, Sichuan University, Chengdu, China

<sup>4</sup> School of Materials Science and Engineering, Nanjing University of Science and Technology, 210094 Nanjing, China

<sup>5</sup> Materials Research Lab at Songshan Lake, 523808 Dongguan, China

a) Electronic mail: zhili@njust.edu.cn

b) Electronic mail: dengzheng@iphy.ac.cn

c) Electronic mail: Jin@iphy.ac.cn

Chemical pressure is an effective method to tune physical properties, particularly for diluted magnetic semiconductors (DMS) of which ferromagnetic ordering is mediated by charge carriers. Via substitution of smaller Ca for larger Sr, we introduce chemical pressure on (Sr,Na)(Cd,Mn)<sub>2</sub>As<sub>2</sub> to fabricate a new DMS material (Ca,Na)(Cd,Mn)<sub>2</sub>As<sub>2</sub>. Carriers and spins are introduced by substitutions of (Ca,Na) and (Cd,Mn) respectively. The unit cell volume reduces by 6.2% after complete substitution of Ca for Sr, suggesting a subsistent chemical pressure. Importantly the local geometry of [Cd/MnAs<sub>4</sub>] tetrahedron is optimized via chemical compression that increases the Mn-As hybridization leading to enhanced ferromagnetic interactions. As a result, the maximum Curie temperature ( $T_C$ ) is increased by about 50% while the the maximum saturation moment increases by over 100% from (Sr,Na)(Cd,Mn)<sub>2</sub>As<sub>2</sub> to (Ca,Na)(Cd,Mn)<sub>2</sub>As<sub>2</sub>. The chemical pressure estimated from the equation of state is equal to an external physical pressure of 3.6 GPa.

The diluted magnetic semiconductors (DMS) have been investigated extensively as they offer an opportunity to control the ferromagnetic properties by changing carrier density. The advantage leads to potential applications in spintronic devices.<sup>1-3</sup> Specifically, recently couples of Fe-doped III-V DMS reached relatively high Curie temperature ( $T_C \sim 320-340$  K),<sup>4-6</sup> which challenges existing concepts and motivates further understanding of ferromagnetism in DMS. The spin & charge doping are induced by one element doping such as Mn doping into (Ga,Mn)As leading to difficulty in tuning either conducting or magnetic properties.<sup>7</sup> Consequently a series of new type of DMS materials with independent carrier and spin doping have been discovered to overcome aforementioned difficulty, e.g.  $\text{Li}_{1+x}(\text{Zn,Mn})\text{As}$  termed “111” type or  $(\text{Ba,K})(\text{Zn,Mn})_2\text{As}_2$  (BZA) termed “122” type. BZA holds the record of Curie temperature (230 K) among the “111” and “122” -type DMS.<sup>7-11</sup>

Given a DMS material, effective ways to modify  $T_C$  can be achieved by increasing the carrier density using an applied electric field, photo excitations or pressure.<sup>7,12</sup> Particularly, pressure is expected to increase both carrier concentration and Mn-As hybridization which result in an enhancement of ferromagnetic interactions in DMS materials.<sup>13</sup> On the other hand, internal chemical pressure which plays a comparable role as external physical pressure, is widely used to modify physical properties in many functional materials. For instance, an equivalent increase in superconducting critical temperature in cuprate superconductors has been reported via relatively low pressures (4-6 GPa) induced by chemical pressure.<sup>14,15</sup> Superconductivity in iron-based compound  $\text{BaFe}_2\text{As}_2$  can be induced by moderate pressure (<6 GPa) and iso-valent chemical doping ( $\text{BaFe}_2\text{As}_{2-x}\text{P}_x$ ) respectively.<sup>16,17</sup> Comparing to external physical pressure, internal chemical pressure which can be applied by iso-valent substitutions, does not require any specific devices (e.g. diamond

anvil cell or piston cylinder cell). Nevertheless, chemical pressure-effects in DMS materials are rarely reported.

Previous studies of physical pressure-effects on “122” BZA only presented negative pressure-effect on  $T_C$ . The proposed reason is that physical pressure distorts  $[\text{MnAs}_4]$  tetrahedra and then reduces effective Mn-As hybridization which in turn damages ferromagnetic ordering.<sup>18-20</sup> In this work we generated chemical pressure by changing atom size on another group of DMS  $(\text{Sr,Na})(\text{Cd,Mn})_2\text{As}_2$ .<sup>21</sup> By replacement of Sr for Ca,  $(\text{Ca,Na})(\text{Cd,Mn})_2\text{As}_2$  was synthesized as a new DMS material. From Sr- to Ca-compound, the unit cell volume decreases by 6.2% suggesting positive chemical pressure effect. It is found that local geometry of  $[\text{MnAs}_4]$  tetrahedron in  $(\text{Ca,Na})(\text{Cd,Mn})_2\text{As}_2$  is optimized by chemical pressure. Consequently, a successful improvement of ferromagnetic ordering by chemical pressure has been observed: comparing to  $(\text{Sr,Na})(\text{Cd,Mn})_2\text{As}_2$ , both maximum Curie temperature and saturation moment in  $(\text{Ca,Na})(\text{Cd,Mn})_2\text{As}_2$  are significantly enhanced.

Polycrystalline samples of  $(\text{Ca,Na})(\text{Cd,Mn})_2\text{As}_2$  were synthesized by solid state reaction with high purity elements. The stoichiometric ratios of starting materials were well mixed and pressed into pellets. All the processes were conducted under the protection of high-purity Argon due to the air-sensitive starting materials. The pellets were sealed in tantalum-tubes with 1 bar of Argon, and then the Ta-tubes were enclosed into evacuated quartz tubes. The samples were firstly heated at 600 °C for 12 hours. Then the products were reground & pelleted, and sintered at 650 °C for another 12 hours. The recovered samples were characterized by powder X-ray diffraction (PXRD) with a Rigaku diffractometer using Cu-K $\alpha$  radiation at room-temperature. Scanning Electron Microscope (SEM) was used to investigate the morphology and particle size.

Real compositions of all the elements were measured with energy dispersive analysis (EDX) on the SEM. The real atom ratios of our samples are consistent with their normal stoichiometry. For example real composition of nominal  $(\text{Ca}_{0.95}\text{Na}_{0.05})(\text{Cd}_{0.95}\text{Mn}_{0.05})_2\text{As}_2$  is determined as  $(\text{Ca}_{0.9546}\text{Na}_{0.0454})(\text{Cd}_{0.9396}\text{Mn}_{0.0604})_2\text{As}_2$ . Consequently we use normal composition of each sample in this manuscript, for the sake of simplification. The *dc* magnetic properties were measured with a Superconductivity Quantum Interference Device (SQUID, Quantum Design), and transport properties were examined by Physical Property Measurement System (PPMS, Quantum design). We calculated the equation of state (EoS) equation by first-principles calculations with plane augmented-wave (PW) pseudopotential and generalized gradient approximation implemented in VASP code with  $16 \times 16 \times 8$  k-point grid and 500 eV energy cutoff to build up relationship between cell volume and pressure ( $P(V)$ ) of  $\text{SrCd}_2\text{As}_2$ .

Both  $\text{CaCd}_2\text{As}_2$  and  $\text{SrCd}_2\text{As}_2$  crystallize into hexagonal structure with  $P-3m1$  space group (No. 164) as shown in Figure 1(a). Powder X-ray diffraction patterns for samples show that all of the peaks can be well indexed into  $P-3m1$  space group (Figure S1). For all the samples, crystal grain has sharp boundaries indicating good crystallization as shown in Figure 1(b). The lattice constants were calculated by Rietveld refinement. Both of *a*- and *c*-axis shrink linearly with increasing Mn doping level in Figure 1(c) because  $\text{Mn}^{2+}$  (0.66 Å) is smaller than  $\text{Cd}^{2+}$  (0.78 Å), well following the Vegard Law, an evidence of successful (Cd,Mn) substitution.  $\text{CaCd}_2\text{As}_2$  and  $\text{SrCd}_2\text{As}_2$  are quasi 2D-materials where Ca/Sr ions layers and honeycomb-like  $\text{Cd}_2\text{As}_2$  layers stack alternately along *c* axis.<sup>22</sup> Given lattice constants for  $\text{SrCd}_2\text{As}_2$  ( $a \sim 4.4516$  Å,  $c \sim 7.4221$  Å,  $V \sim 127.4$  Å<sup>3</sup>) and  $\text{CaCd}_2\text{As}_2$  ( $a \sim 4.3909$  Å,  $c \sim 7.1870$  Å,  $V \sim 120.0$  Å<sup>3</sup>), chemical compression effect is visible in the latter, particularly

along c-axis. Besides, two more principal deviations between  $\text{CaCd}_2\text{As}_2$  and  $\text{SrCd}_2\text{As}_2$  is the Cd/Mn-As bond lengths and As-Cd/Mn-As bond angles in  $\text{Cd}_2\text{As}_2$  layers which will be discussed in more details.

Figure 2(a) shows temperature dependent of magnetization ( $M(T)$ ) curves for  $(\text{Ca}_{1-x}\text{Na}_x)(\text{Cd}_{1-y}\text{Mn}_y)_2\text{As}_2$  ( $x = 0.025, 0.05, 0.1, 0.15$ ;  $y = 0.05, 0.15, 0.2$ ) under field  $H = 500$  Oe. There is no obvious difference between zero field cooling (ZFC) and field cooling (FC) but clear ferromagnetic signatures are observed for all samples, i.e. sharp upturns with decreasing temperature.  $T_C$  were determined from valleys of  $dM/dT$  curves. Above  $T_C$ , susceptibility is fitted with Curie-Weiss law (inset of Figure 2(a)),  $(\chi - \chi_0)^{-1} = (T - \theta)/C$ , where  $\chi_0$  stands for a temperature-independent term and  $\theta$  for paramagnetic temperature. Neither  $T_C$  nor  $\theta$  monotonically increases with increasing Mn or Na doping level (Figure 2(c)). Maximum  $T_C \sim 19$  K and  $\theta \sim 22$  K are obtained for  $x = 0.05, y = 0.15$ . The maximum  $T_C$  of  $(\text{Ca,Na})(\text{Cd,Mn})_2\text{As}_2$  is about 50% higher than that of  $(\text{Sr,Na})(\text{Cd,Mn})_2\text{As}_2$  (the maximum  $T_C \sim 13$  K).<sup>21</sup> In Figure 2(c)  $T_C$  decreases slightly with higher Na-doping level when  $x > 0.05$ , is presumable due to more defects induced by Na doping in specimens. After reaching maximum  $T_C$ , ferromagnetic ordering is also weakened by over-doped Mn, similar to analogues  $(\text{Sr,Na})(\text{Zn,Mn})_2\text{As}_2$  and  $(\text{Sr,Na})(\text{Cd,Mn})_2\text{As}_2$ .<sup>21,23</sup> A presumably reason is that increasing chemical substitution tends to enhance antiferromagnetic coupling between either substitutional Mn and interstitial Mn or substitutional Mn in the nearest neighbor Cd sites, due to high Mn concentration. Effective paramagnetic moments ( $M_{\text{eff}}$ ) are calculated from the Curie constant  $C$ . For example  $M_{\text{eff}}$  of

$(\text{Ca}_{0.95}\text{Na}_{0.05})(\text{Cd}_{0.95}\text{Mn}_{0.05})_2\text{As}_2$  is  $5.3 \mu_B/\text{Mn}$  which is close to expected value of  $s = 5/2$  configuration of  $\text{Mn}^{2+}$  ( $g\sqrt{s(s+1)} = 5.9\mu_B$  with  $g = 2$ ). Ferromagnetic characteristics, which are spontaneous magnetization under very low fields, narrow but clear hysteresis loops, are also found in  $M(H)$  curves as plotted in Figure 2(b). Coercive fields are smaller than 100 Oe. Saturation moments ( $M_{\text{sat}}$ ) decrease with increasing Mn (Figure 2(d)), due to increased antiferromagnetic interactions as proposed to explain the decrease of  $T_C$ . Nevertheless, maximum  $M_{\text{sat}}$  of  $(\text{Ca},\text{Na})(\text{Cd},\text{Mn})_2\text{As}_2$  is significant larger than that of  $(\text{Sr},\text{Na})(\text{Cd},\text{Mn})_2\text{As}_2$  (Maximum  $M_{\text{sat}} < 1\mu_B/\text{Mn}$ ). The larger  $M_{\text{sat}}$  indicates that more local spins on Mn are ferromagnetic ordered, consistent with higher  $T_C$  in  $(\text{Ca},\text{Na})(\text{Cd},\text{Mn})_2\text{As}_2$ .<sup>21</sup>

Electrical transport measurements are shown in Figure 3. The temperature dependent resistivity ( $\rho(T)$ ) for parent compound  $\text{CaCd}_2\text{As}_2$  shows semiconducting behavior within temperature range of 2 – 300 K (Figure 3(a)). It is worth noting that the resistivity of  $\text{CaCd}_2\text{As}_2$  is much smaller than  $\text{SrCd}_2\text{As}_2$  ( $\rho_{300\text{K}} \sim 1*10^4 \Omega\cdot\text{mm}$  and  $\rho_{120\text{K}} \sim 1*10^7 \Omega\cdot\text{mm}$ ).<sup>21</sup> It is consistent with the aforementioned scenario that shortened Cd/Mn-As bond lengths and optimized As-Zn/Mn-As bond angle within sub-layers enhance intra-sub-layer Cd/Mn-As hybridization and in turn benefit conduction. On the other hand,  $\rho_{2\text{K}}$  of  $\text{CaCd}_2\text{As}_2$  is 3 orders magnitude larger than all the Na-doped  $(\text{Ca},\text{Na})(\text{Cd},\text{Mn})_2\text{As}_2$ , indicating significantly increased carrier concentrations via Na doping. The scheme is further supported as shown in Figure 3(a) by the decrease of resistivity of  $(\text{Ca}_{1-x}\text{Na}_x)(\text{Cd}_{0.85}\text{Mn}_{0.15})_2\text{As}_2$  with increasing Na-doping level. In contrast, as shown in Figure 3(b), resistivity of  $(\text{Ca}_{0.95}\text{Na}_{0.05})(\text{Cd}_{1-y}\text{Mn}_y)_2\text{As}_2$  gradual increases with increasing Mn concentrations.

Figure 4(a) shows  $\rho(T)$  curves for  $(\text{Ca}_{0.95}\text{Na}_{0.05})(\text{Cd}_{0.85}\text{Mn}_{0.15})_2\text{As}_2$  under various fields. Negative magnetoresistance ( $\text{MR} = \Delta\rho/\rho_0 = (\rho_H - \rho_0)/\rho_0$ ) is found below  $\sim 18$  K consistent with  $T_C$  from magnetization data. Above 18 K, positive MR emerges. The consistency indicates that the negative MR is related to ferromagnetic ordering. In Figure 4(b), MR doesn't saturate at  $H = 7$  T and  $T = 2$  K, where the spins are almost fully aligned according to  $M(H)$  curve. In  $(\text{Ga,Mn})\text{As}$ , and analogue  $(\text{Sr,Na})(\text{Cd,Mn})_2\text{As}_2$  the unsaturated MR are explained with giant splitting of the valence band. In order to understand such behavior, the negative magnetoresistance data at 2 K are fitted with following equation,<sup>24-26</sup>

$$\Delta\rho / \rho_H = \Delta\sigma / \sigma = kB^{1/2} = -n_v e^2 C_0 \rho (eB\hbar)^{1/2} / (2\pi^2 \hbar), \quad (1)$$

Where  $C_0 \approx 0.605$ ,  $e$  is the elemental charge,  $\hbar$  is the reduced Planck constant, respectively, and  $1/2 \leq n_v \leq 2$  depending on the number of hole sub-bands contributing to the charge transport. The best fitting to Eq. (1) gives  $n_v = 0.62$ , close to that of  $(\text{Sr,Na})(\text{Cd,Mn})_2\text{As}_2$ . The maximum MR is  $\sim 15\%$  at  $T = 2$  K and  $H = 7$  T. It is larger than analogues  $(\text{Sr,Na})(\text{Zn,Mn})_2\text{As}_2$  and  $(\text{Ca,Na})(\text{Zn,Mn})_2\text{As}_2$  as well as  $(\text{Ba,K})(\text{Zn,Mn})_2\text{As}_2$  which has a much higher  $T_C$ .<sup>10,27-28</sup>

Carrier type of the parent phase  $\text{CaCd}_2\text{As}_2$  and doped phases  $(\text{Ca,Na})(\text{Cd,Mn})_2\text{As}_2$  is  $p$ -type. The hole concentration of these samples are about  $10^{19}$  -  $10^{20}\text{cm}^{-3}$ . Figure 4(c) shows Hall resistivity ( $\rho_{xy}(H)$ ) below and above  $T_C$  for  $(\text{Ca}_{0.9}\text{Na}_{0.1})(\text{Cd}_{0.85}\text{Mn}_{0.15})_2\text{As}_2$  as a typical example. At  $T = 2$  K, the clear anomalous Hall effect (AHE) is a strong evidence for intrinsic ferromagnetism in a DMS material. Carrier concentration calculated with linear  $\rho_{xy}(H)$  at high-field range is  $n_p = 2.98 \times 10^{19}\text{cm}^{-3}$ . At 300 K  $\rho_{xy}$  is proportional to field and we obtain  $n_p = 5.38 \times 10^{19}\text{cm}^{-3}$ .

Considering key roles of local geometry of  $[\text{Zn/MnAs}]_4$  tetrahedra to ferromagnetic interaction in BZA, we compare Cd/Mn-As bond lengths and As-Cd/Mn-As bond angles of  $\text{CaCd}_2\text{As}_2$  and  $\text{SrCd}_2\text{As}_2$  to seek microscopic insight into the origin of improved ferromagnetic ordering in  $\text{CaCd}_2\text{As}_2$ . For carrier-mediated ferromagnetism in DMS, itinerant carriers play an important role in ferromagnetic interaction.<sup>29-38</sup> Given the quasi 2D structural of  $\text{CaCd}_2\text{As}_2$  and  $\text{SrCd}_2\text{As}_2$ , one can expect carriers are more itinerant along ab-plane than c-axis. If one takes a close look at  $\text{Cd}_2\text{As}_2$  planes, it is easy to find two sub-layers within one CdAs plane (Figure 1 (a)). It is reasonable to assume that intra-sub-layer component is more important than inter-sub-layer one to modify carriers mobility within the  $\text{Cd}_2\text{As}_2$  plane. With the same doping levels, sub-layer of  $\text{CaCd}_2\text{As}_2$  has shorter Cd/Mn-As bond length and more optimal As-Cd/Mn-As bond angles than that of  $\text{SrCd}_2\text{As}_2$ . As shown in Figure 1 (d), the  $(\text{Ca}_{0.95}\text{Na}_{0.05})(\text{Cd}_{0.95}\text{Mn}_{0.05})\text{As}_2$  has the average Cd/Mn-As bond length of 2.700 Å and the average As-Cd/Mn-As bond angle within sub-layers of 108.9° that is close to the ~109.47° for a nondistorted ideal tetrahedron.<sup>18</sup> On the other hand in  $(\text{Sr}_{0.95}\text{Na}_{0.05})(\text{Cd}_{0.95}\text{Mn}_{0.05})\text{As}_2$  the average Cd/Mn-As bond length is 2.712 Å and the average As-Cd/Mn-As bond angle is 113.6° that is apparently deviated from the ~109.47°. The shortened Cd/Mn-As bond length will definitely increase Mn-As hybridization. Additionally the ideal As-Cd/Mn-As bond angle will increase the overlap of Mn-As planar orbitals and guarantee the maximum strength of Mn-As hybridization, hence increasing the ferromagnetic interactions. Previous studies of physical pressure-effects on “122” BZA indicated that shortened Zn/Mn-As bond length and optimized As-Zn/Mn-As bond angle (~109.47° for a regular tetrahedron) will enhance Cd/Mn-As hybridization.<sup>18</sup> In short  $(\text{Ca,Na})(\text{Cd,Mn})_2\text{As}_2$  have stronger intra-sub-layer Cd/Mn-As hybridization than that for  $(\text{Sr,Na})(\text{Cd,Mn})_2\text{As}_2$ . As a result,

we found improved ferromagnetic ordering in  $(\text{Ca,Na})(\text{Cd,Mn})_2\text{As}_2$ . Consequently, it is reasonable to assume more chemical pressure could further improve  $T_c$  within this system. We suggest replacing Ca with Mg for future investigation, due to smaller cation size of Mg.

We calculated the equation of state (EoS) equation with first-principles calculations with plane augmented-wave (PW) pseudopotential method implemented in VASP code<sup>39</sup> to build up relationship between cell volume and pressure ( $P(V)$ ) of  $\text{SrCd}_2\text{As}_2$  (Figure S2). Based on  $P(V)$  curve, we estimate that an external pressure of 3.6 GPa can reduce cell volume of  $\text{SrCd}_2\text{As}_2$  to  $120.0 \text{ \AA}^3$  (volume of  $\text{CaCd}_2\text{As}_2$  at ambient pressure).

In summary, we successfully synthesized a new type of DMS,  $(\text{Ca,Na})(\text{Cd,Mn})_2\text{As}_2$ . The carriers and spins are introduced via (Ca,Na) and (Cd, Mn) substitutions independently. The Curie temperature of  $(\text{Ca,Na})(\text{Cd,Mn})_2\text{As}_2$  is 50% higher than that for  $(\text{Sr,Na})(\text{Cd,Mn})_2\text{As}_2$  due to the effects of chemical pressure, and the saturation moments is also enhanced dramatically. The significant improvement of ferromagnetism in  $(\text{Ca,Na})(\text{Cd,Mn})_2\text{As}_2$  indicate the prospect to search for high temperature diluted magnetic semiconductors via proper chemical pressure.

## Supplementary Material

See supplementary material for the PXRD pattern of  $(\text{Ca}_{0.95}\text{Na}_{0.05})(\text{Cd}_{1-y}\text{Mn}_y)_2\text{As}_2$  ( $y = 0, 0.05, 0.1, 0.15$  and  $0.2$ ) and the calculated  $P(V)$  of  $\text{SrCd}_2\text{As}_2$

## Acknowledgments

This work was financially supported by National Key R&D Program of China (No. 2017YFB0405703), Ministry of Science and Technology of China

(2018YFA03057001) & National Natural Science Foundation of China through the research projects(11534016).

## References

- <sup>1</sup>I. Zutic, J. Fabian, and S. Das Sarma, *Rev. Mod. Phys.* **76**, 323 (2004).
- <sup>2</sup>T. Jungwirth, J. Wunderlich, V. Novak, K. Olejnik, B. L. Gallagher, R. P. Campion, K. W. Edmonds, A. W. Rushforth, A. J. Ferguson, and P. Nemeč, *Rev. Mod. Phys.* **86**, 855 (2014).
- <sup>3</sup>H. Ohno, *Science* **281**, 951 (1998).
- <sup>4</sup>N. T. Tu, P. N. Hai, L. D. Anh, and M. Tanaka, *Appl. Phys. Lett.* **108**, 192401 (2016).
- <sup>5</sup>N. T. Tu, P. N. Hai, L. D. Anh, and M. Tanaka, *Appl. Phys. Express* **11**, 063005 (2018)
- <sup>6</sup>N. T. Tu, P. N. Hai, L. D. Anh, and M. Tanaka, *Appl. Phys. Lett.* **112**, 122409 (2018)
- <sup>7</sup>A. Hirohata, H. Sukegawa, H. Yanagihara, I. Zutic, T. Seki, S. Mizukami, and R. Swaminathan, *IEEE Trans. Magn.* **51**, 0800511 (2015).
- <sup>8</sup>I. Zutic and T. Zhou, *Sci. China. Phys. Mech.* **61**, 067031 (2018).
- <sup>9</sup>J. K. Glasbrenner, I. Zutic, and I. I. Mazin, *Phys. Rev. B* **90**, 140403 (2014).
- <sup>10</sup>K. Zhao, Z. Deng, X. C. Wang, W. Han, J. L. Zhu, X. Li, Q. Q. Liu, R. C. Yu, T. Goko, B. Frandsen, Lian Liu, Fanlong Ning, Y. J. Uemura, H. Dabkowska, G. M. Luke, H. Luetkens, E. Morenzoni, S. R. Dunsiger, A. Senyshyn, P. Böni, and C. Q. Jin, *Nat. Commun.* **4**, 1442 (2013).
- <sup>11</sup>K. Zhao, B. J. Chen, G. Q. Zhao, Z. Yuan, Q. Q. Liu, Z. Deng, J. L. Zhu, and C. Q. Jin, *Chin. Sci. Bull.* **59**, 2524 (2014).
- <sup>12</sup>H. Ohno, D. Chiba, F. Matsukura, T. Omiya, E. Abe, T. Dietl, Y. Ohno, and K. Ohtani, *Nature* **408**, 944 (2000).
- <sup>13</sup>M. Csontos, G. Mihaly, B. Janko, T. Wojtowicz, X. Liu, and J. K. Furdyna, *Nat. Mater.* **4**, 447 (2005).
- <sup>14</sup>M. Almamouri, P. P. Edwards, C. Greaves, and M. Slaski, *Nature* **369**, 382 (1994).
- <sup>15</sup>W. B. Gao, Q. Q. Liu, L. X. Yang, Y. Yu, F. Y. Li, C. Q. Jin and S. Uchida, *Phys. Rev. B* **80**, 094523 (2009)
- <sup>16</sup>S. Kasahara, T. Shibauchi, K. Hashimoto, K. Ikada, S. Tonegawa, R. Okazaki, H. Shishido, H. Ikeda, H. Takeya, K. Hirata, T. Terashima, and Y. Matsuda, *Phys. Rev. B* **81**, 184519 (2010).
- <sup>17</sup>S. A. J. Kimber, A. Kreyssig, Y. Z. Zhang, H. O. Jeschke, R. Valenti, F. Yokaichiya, E. Colombier, J. Yan, T. C. Hansen, T. Chatterji, R. J. McQueeney, P. C. Canfield, A. I. Goldman, and D. N. Argyriou, *Nat. Mater.* **8**, 471 (2009).
- <sup>18</sup>F. Sun, G. Q. Zhao, C. A. Escanhoela, B. J. Chen, R. H. Kou, Y. G. Wang, Y. M. Xiao, P. Chow, H. K. Mao, D. Haskel, W. G. Yang, and C. Q. Jin, *Phys. Rev. B* **95**, 094412 (2017).
- <sup>19</sup>G. Q. Zhao, Z. Li, F. Sun, Z. Yuan, B. J. Chen, S. Yu, Y. Peng, Z. Deng, X. C. Wang, and C. Q. Jin, *J. Phys-Condens. Mat.* **30**, 254001 (2018).
- <sup>20</sup>F. Sun, N. N. Li, B. J. Chen, Y. T. Jia, L. J. Zhang, W. M. Li, G. Q. Zhao, L. Y. Xing, G. Fabbris, Y. G. Wang, Z. Deng, Y. J. Uemura, H. K. Mao, D. Haskel, W. G. Yang, and C. Q. Jin, *Phys. Rev. B* **93**, 224403 (2016).
- <sup>21</sup>B. J. Chen, Z. Deng, W. M. Li, M. R. Gao, Z. Li, G. Q. Zhao, S. Yu, X. C. Wang, Q. Q. Liu, and C. Q. Jin, *J. Appl. Phys.* **120**, 083902 (2016).
- <sup>22</sup>P. Klufers and A. Mewis, *Z. Naturforsch., B: Chem. Sci.* **32**, 753 (1977).
- <sup>23</sup>Xiaojun Yang, Yuke Li, Pan Zhang, Hao Jiang, Yongkang Luo, Qian Chen, Chunmu Feng, Chao Cao, Jianhui Dai, Qian Tao, Guanghan Cao, and Zhu-An Xu, *J. Appl. Phys.* **114**, 223905 (2013).

- <sup>24</sup>A. Kawabata, *Solid State Commun.* **34**, 431 (1980).
- <sup>25</sup>T. Omiya, F. Matsukura, T. Dietl, Y. Ohno, T. Sakon, M. Motokawa, and H. Ohno, *Physica E* **7**, 976 (2000).
- <sup>26</sup>F. Matsukura, M. Sawicki, T. Dietl, D. Chiba, and H. Ohno, *Physica E* **21**, 1032 (2004).
- <sup>27</sup>B. J. Chen, K. Zhao, Z. Deng, W. Han, J. L. Zhu, X. C. Wang, Q. Q. Liu, B. Frandsen, L. Liu, S. Cheung, F. L. Ning, T. J. S. Munsie, T. Medina, G. M. Luke, J. P. Carlo, J. Munevar, Y. J. Uemura, and C. Q. Jin, *Phys. Rev. B* **90**, 155202 (2014).
- <sup>28</sup>K. Zhao, B. J. Chen, Z. Deng, W. Han, G. Q. Zhao, J. L. Zhu, Q. Q. Liu, X. C. Wang, B. Frandsen, L. Liu, S. Cheung, F. L. Ning, T. J. S. Munsie, T. Medina, G. M. Luke, J. P. Carlo, J. Munevar, G. M. Zhang, Y. J. Uemura, and C. Q. Jin, *J. Appl. Phys.* **116**, 163906 (2014).
- <sup>29</sup>Z. Deng, C. Q. Jin, Q. Q. Liu, X. C. Wang, J. L. Zhu, S. M. Feng, L. C. Chen, R. C. Yu, C. Arguello, T. Goko, F. L. Ning, J. S. Zhang, Y. Y. Wang, A. A. Aczel, T. Munsie, T. J. Williams, G. M. Luke, T. Kakeshita, S. Uchida, W. Higemoto, T. U. Ito, B. Gu, S. Maekawa, G. D. Morris, and Y. J. Uemura, *Nat. Commun.* **2**, 422 (2011).
- <sup>30</sup>Z. Deng, K. Zhao, B. Gu, W. Han, J. L. Zhu, X. C. Wang, X. Li, Q. Q. Liu, R. C. Yu, T. Goko, B. Frandsen, L. Liu, J. S. Zhang, Y. Y. Wang, F. L. Ning, S. Maekawa, Y. J. Uemura, and C. Q. Jin, *Phys. Rev. B* **88**, 081203 (2013).
- <sup>31</sup>R. Wang, Z. X. Huang, G. Q. Zhao, S. Yu, Z. Deng, C. Q. Jin, Q. J. Jia, Y. Chen, T. Y. Yang, X. M. Jiang, and L. X. Cao, *AIP Adv.* **7**, 045017 (2017).
- <sup>32</sup>G. Q. Zhao, C. J. Lin, Z. Deng, G. X. Gu, S. Yu, X. C. Wang, Z. Z. Gong, Y. J. Uemura, Y. Q. Li, and C. Q. Jin, *Sci. Rep.* **7**, 14473 (2017).
- <sup>33</sup>C. Ding, H. Y. Man, C. Qin, J. C. Lu, Y. L. Sun, Q. Wang, B. Q. Yu, C. M. Feng, T. Goko, C. J. Arguello, L. Liu, B. A. Frandsen, Y. J. Uemura, H. D. Wang, H. Luetkens, E. Morenzoni, W. Han, C. Q. Jin, T. Munsie, T. J. Williams, R. M. D'Ortenzio, T. Medina, G. M. Luke, T. Imai, and F. L. Ning, *Phys. Rev. B* **88**, 041102 (2013).
- <sup>34</sup>W. Han, K. Zhao, X. C. Wang, Q. Q. Liu, F. L. Ning, Z. Deng, Y. Liu, J. L. Zhu, C. Ding, H. Y. Man, and C. Q. Jin, *Sci. China. Phys. Mech.* **56**, 2026 (2013).
- <sup>35</sup>H. Y. Man, S. L. Guo, Y. Sui, Y. Guo, B. Chen, H. D. Wang, C. Ding, and F. L. Ning, *Sci. Rep.* **5**, 15507 (2015).
- <sup>36</sup>F. Sun, C. Xu, S. Yu, B. J. Chen, G. Q. Zhao, Z. Deng, W. G. Yang, and C. Q. Jin, *Chin. Phys. Lett.* **34**, 067501 (2017).
- <sup>37</sup>B. A. Frandsen, Z. Z. Gong, M. W. Terban, S. Banerjee, B. J. Chen, C. Q. Jin, M. Feyngenson, Y. J. Uemura, and S. J. L. Billinge, *Phys. Rev. B* **94**, 094102 (2016).
- <sup>38</sup>S. C. Erwin and I. Zutic, *Nat. Mater.* **3**, 410 (2004).
- <sup>39</sup>G. Kresse and D. Joubert, *Phys. Rev. B* **59** (3), 1758 (1999).

## Figure Caption

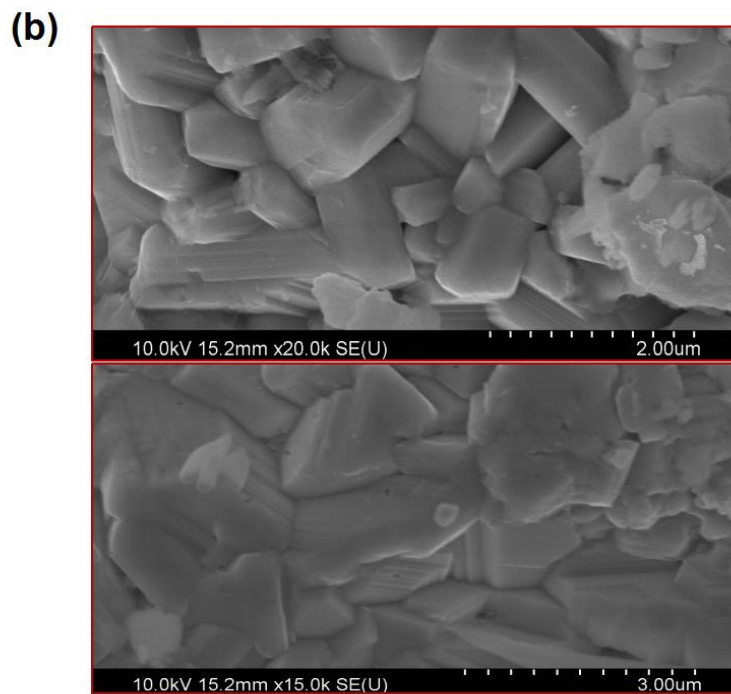
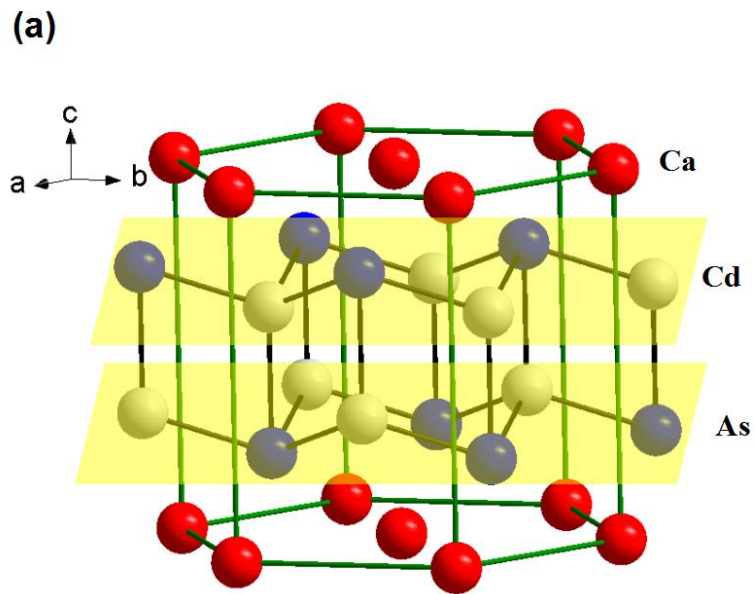
Figure 1. (a) Crystal structure of the parent phase,  $\text{CaCd}_2\text{As}_2$ . The CdAs sub-layers are highlighted with yellow parallelograms. (b) SEM images of  $(\text{Ca}_{0.95}\text{Na}_{0.05})(\text{Cd}_{0.9}\text{Mn}_{0.1})_2\text{As}_2$ . (c) Lattice constants versus Mn doping levels. (d)  $[\text{Cd}/\text{MnAs}]_4$  tetrahedra in  $(\text{Ca}_{0.95}\text{Na}_{0.05})(\text{Cd}_{0.95}\text{Mn}_{0.05})\text{As}_2$  and  $(\text{Sr}_{0.95}\text{Na}_{0.05})(\text{Cd}_{0.95}\text{Mn}_{0.05})\text{As}_2$ . Marked bond length and bond angle are the ones within the CdAs sub-layers.

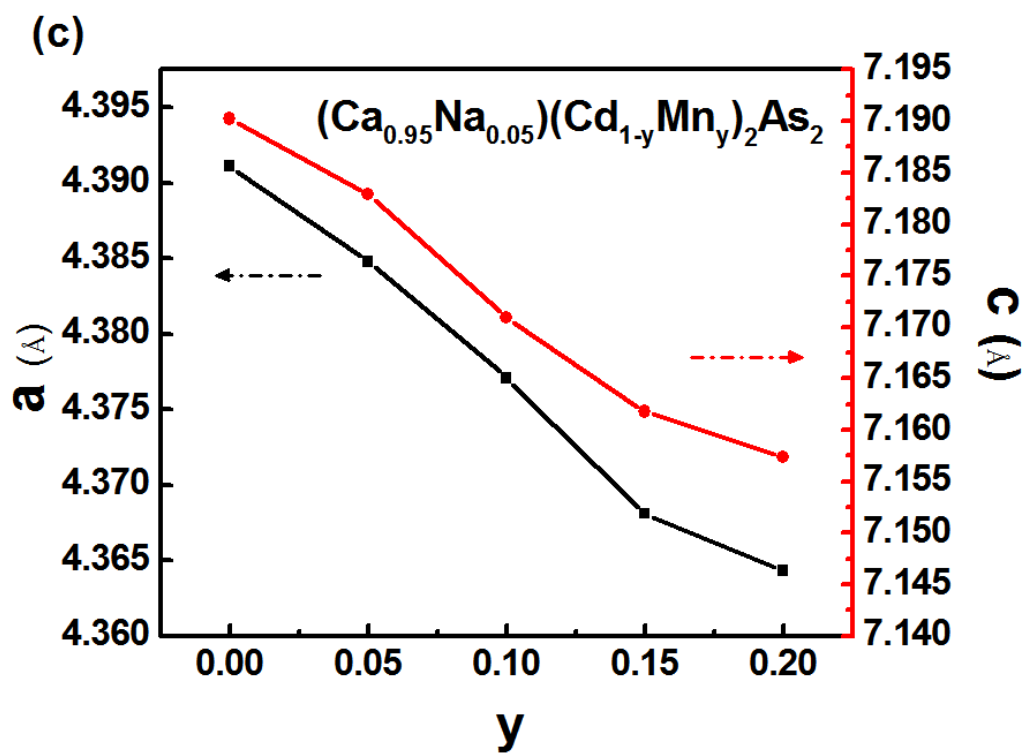
Figure 2. (a)  $M(T)$  measured under  $H = 500$  Oe of  $(\text{Ca}_{1-x}\text{Na}_x)(\text{Cd}_{1-y}\text{Mn}_y)_2\text{As}_2$  ( $x = 0.025, 0.05, 0.1, 0.15$ ;  $y = 0.05, 0.15, 0.2$ ). (b) The hysteresis loops at 2 K for  $(\text{Ca}_{1-x}\text{Na}_x)(\text{Cd}_{1-y}\text{Mn}_y)_2\text{As}_2$  ( $x = 0.025, 0.05, 0.1, 0.15$ ;  $y = 0.05, 0.15, 0.2$ ). (c)  $T_C$  and  $\theta$  versus Na- and Mn doping level. (d)  $M_{\text{sat}}$  versus Mn doping level.

Figure 3. Temperature dependent resistivity curves of (a)  $(\text{Ca}_{1-x}\text{Na}_x)(\text{Cd}_{0.85}\text{Mn}_{0.15})_2\text{As}_2$ , ( $x = 0.025, 0.05, 0.1$ ) and  $\text{CaCd}_2\text{As}_2$  in the insert. (b)  $(\text{Ca}_{0.95}\text{Na}_{0.05})(\text{Cd}_{1-y}\text{Mn}_y)_2\text{As}_2$  ( $y = 0.05, 0.15, 0.2$ ).

Figure 4. (a)  $\rho(T)$  curves of  $(\text{Ca}_{0.95}\text{Na}_{0.05})(\text{Cd}_{0.85}\text{Mn}_{0.15})_2\text{As}_2$  under various field. (b) Magnetoresistance curves of  $(\text{Ca}_{0.95}\text{Na}_{0.05})(\text{Cd}_{0.85}\text{Mn}_{0.15})_2\text{As}_2$  measured in an external field up to 7 T at  $T = 2, 10, 20,$  and  $50$  K, respectively. The pink circles show the fitting result according to Eq. (1). (c) Hall effect measurement results for  $(\text{Ca}_{0.9}\text{Na}_{0.1})(\text{Cd}_{0.85}\text{Mn}_{0.15})_2\text{As}_2$ . The inset shows AHE and hysteresis loop in the low-field region.

**Figure 1**





(d)

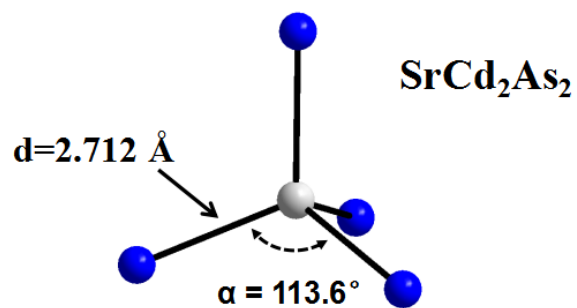
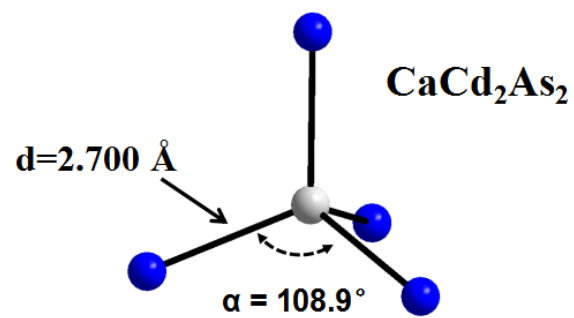
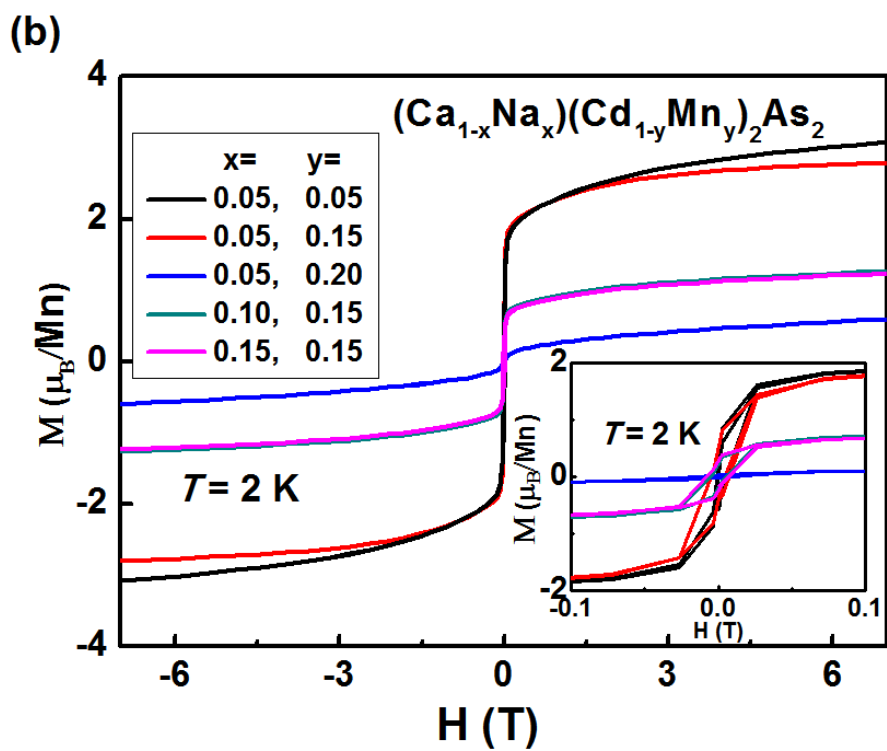
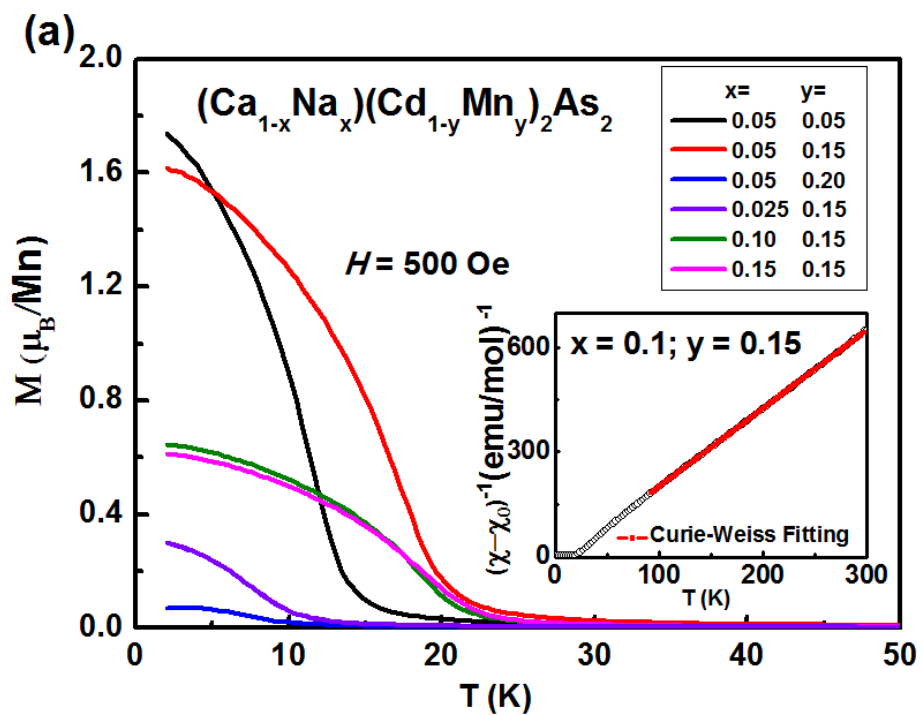


Figure 2



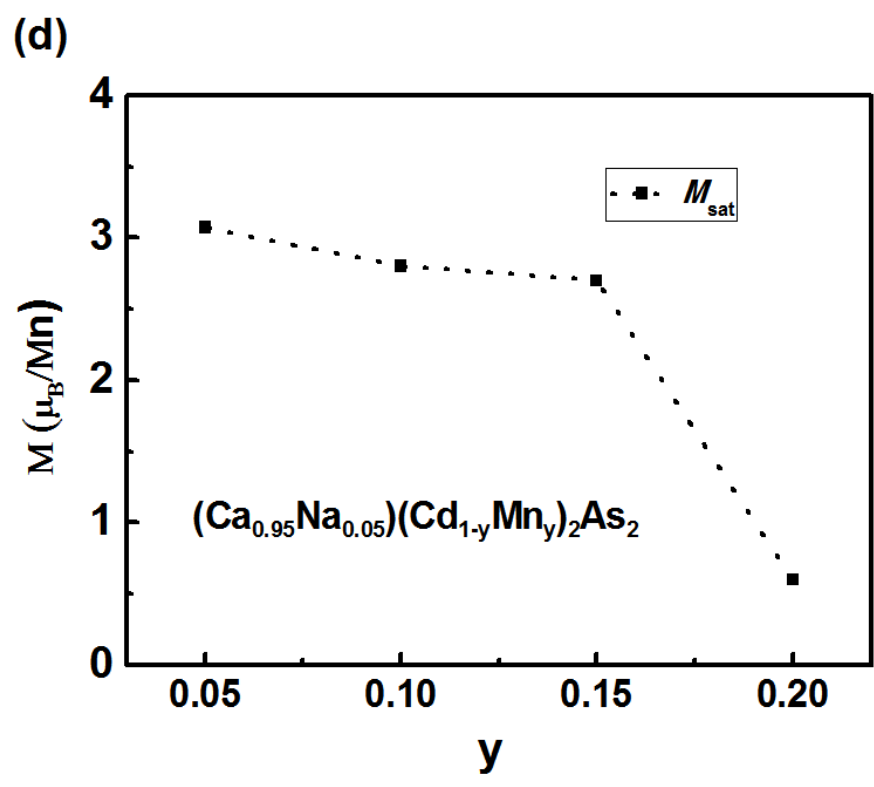
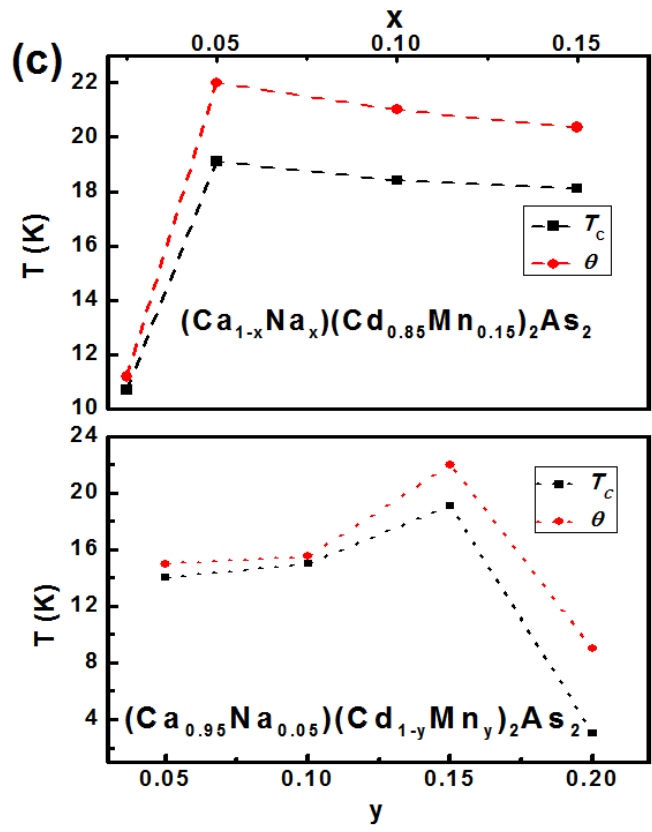
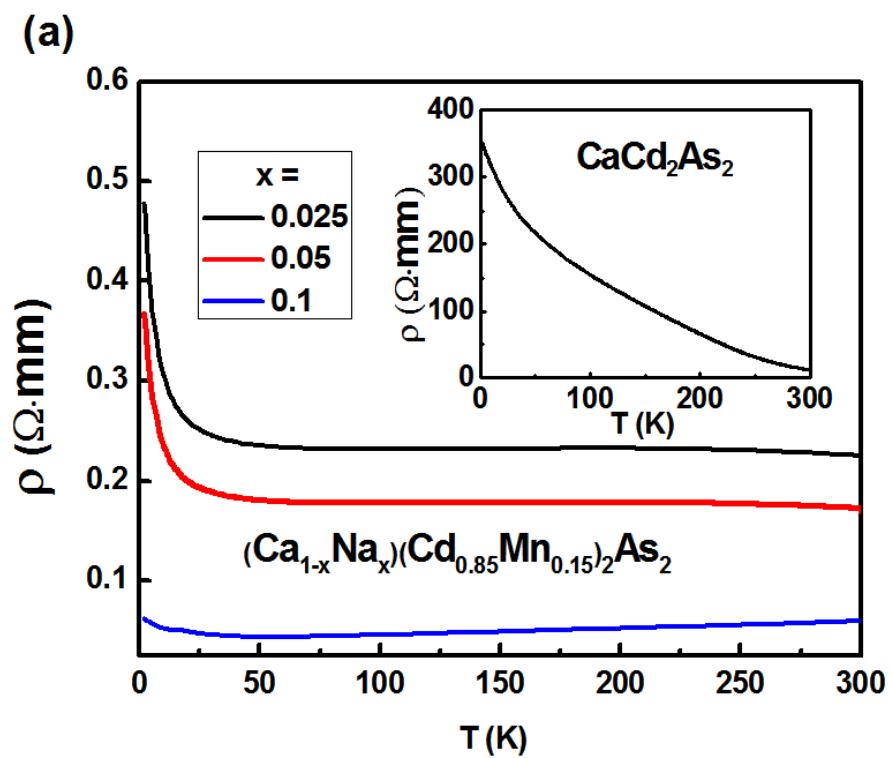


Figure 3



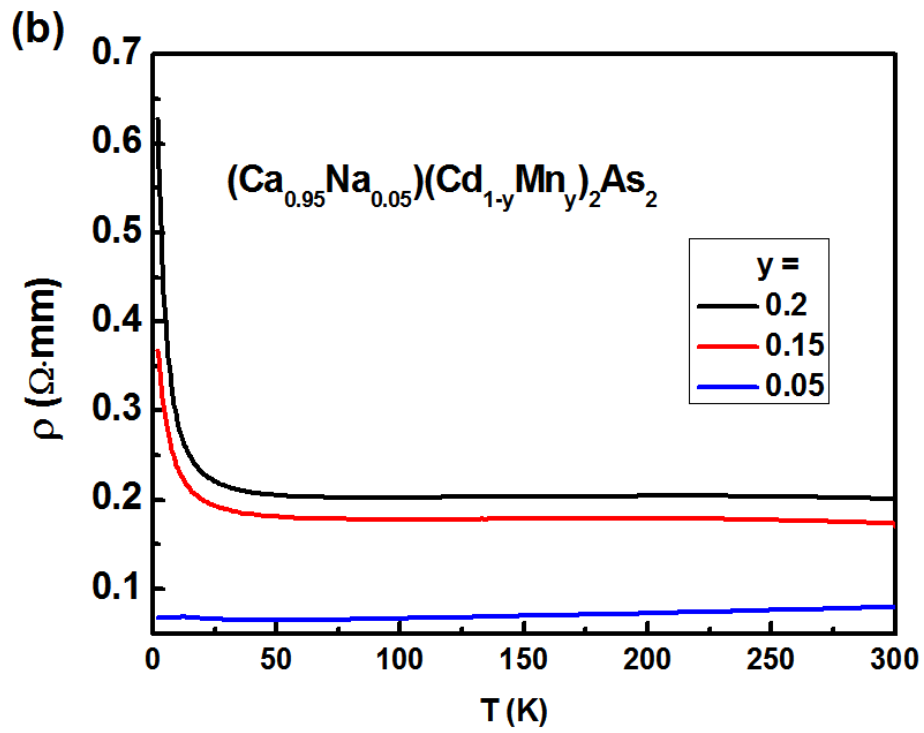


Figure 4

